IET Optoelectronics

WILEY

The Institution of Engineering and Technology

ORIGINAL RESEARCH OPEN ACCESS

Channel Characterisation for Underwater Optical Wireless Vertical Links

Alessandro Ugolini[1,2] | Federica Poli[1,2] | Daniele Croce[2,3] | Stefano Mangione[2,3]

[1]Department of Engineering and Architecture, University of Parma, Parma, Italy | [2]National Inter-University Consoritum for Telecommunications, CNIT, Parma, Italy | [3]Department of Engineering, University of Palermo, Palermo, Italy

Correspondence: Alessandro Ugolini (alessandro.ugolini@unipr.it)

Received: 20 December 2024 | **Revised:** 28 March 2025 | **Accepted:** 2 June 2025

Handling Editor: Mónica Figueiredo

Funding: This research was funded by the European Union under the Italian National Recovery and Resilience Plan (NRRP) of NextGenerationEU: Partnership on 'Telecommunications of the Future' (PE00000001—program 'RESTART'), projects S10—SEXTET, CUP E63C22002070006, and S14—Net4Future, CUP D93C22000910001.

Keywords: underwater optical wireless communications | vertical links | visible light communication | water channel characterization | wavelength division multiplexing technology

ABSTRACT

We provide a detailed description of depth-dependent effects that affect the propagation of light in underwater optical wireless communication links. Absorption and scattering properties of water are evaluated for realistic chlorophyll profiles versus depth for all the visible spectrum, with particular attention to the wavelengths corresponding to practically feasible laser sources. Results show which visible wavelength is the less affected by propagation loss in specific water conditions, thus being the most suitable to improve the performance of vertical links in underwater optical wireless communications. The developed model is useful also to optimise the distribution of optical channels in systems based on dense wavelength division multiplexing technology, according to the type of water and the depth reached in the vertical communication link.

1 | Introduction

Underwater optical wireless communications (UOWC) have raised an increasing interest for different applications, such as environmental monitoring, exploration, security, and defence [1–3], and are emerging as the new frontier for 6G and beyond networks [4]. In this scenario, it is of great importance to develop reliable models of the underwater optical wireless channel, in order to realistically evaluate the performance of the proposed solutions.

A common model for the underwater optical channel relies on the classification of water based on its purity or turbidity [5, 6], by defining four water types, each associated with a set of values for the parameters describing absorption and scattering phenomena that affect the light propagation. Although this model is simple and easy to apply, it is mostly well suited for horizontal links (i.e., when transmitter and receiver are at the same depth). In fact, it does not take into account variations in the water characteristics which happen when changing depth. Disregarding these effects can lead to incorrect conclusions when the transmission crosses multiple layers of water with different properties. For these reasons more realistic models, taking into account depth-dependent water characteristics, have been proposed in the literature [7–10].

Commonly adopted solutions using visible light in underwater optical wireless links are based on blue and green lasers to exploit the relatively low absorption affecting the propagation of light in the wavelength range from 450 to 550 nm [11, 12]. In

particular, most works in the literature adopt a green source, operating at a wavelength around 532 nm. This choice is convenient not only for the performance improvement of UOWC links, since green light is one of the less affected by absorption in the water, but also for the system implementation, given the availability of reliable green lasers. However, for a detailed description of light transmission in the water, absorption should be considered together with other impairments. Moreover, it is necessary to analyse how all these phenomena are influenced by light wavelength, water properties, especially its level of turbidity, and depth [9, 13]. Hence, the selection of green as the operating wavelength for UOWCs should not be taken for granted. A comprehensive analysis of light propagation underwater, taking into account all the cited factors, can provide more precise information about the most suitable wavelength to use for the communication link, which should be combined with the availability of optical sources and detectors. Recently, new visible fibre lasers have been demonstrated in literature [14–16]. For example, a novel cyan laser has been proposed as a feasible option for UOWC [14]. Moreover, a cost effective dense wavelength division multiplexing (WDM) emitter, made by combining seven lasers in the blue-green range with a fine wavelength spacing of 2 nm, has been proposed [12]. The WDM technology, already widely used in fibre-based and free-space optical communication systems, can be successfully exploited also for UOWC [17], in particular for turbidity-tolerant high-speed communication links [12].

In this paper, we study the behaviour of a vertical underwater link when visible light is transmitted. We express in a unified framework the main wavelength- and depth-dependent effects that characterise light propagation in water. The influence of wind-induced air bubbles and foam [18] has been neglected, being its impact on light propagation limited, even in the presence of strong wind, and not wavelength-dependent [19]. Also the seawater refractive index changes as a function of salinity and temperature [20] have not been included in the framework, since these variations are not significant in the intervals of depth relevant for UOWCs [21]. Notice that all the effects mentioned up to now are directly related to the physical properties of the transmission medium, that is seawater. Other impairments more related to its stochastic behaviour, such as turbulence [22] and pointing errors due to random movements of the waves at the sea surface [23, 24], are neglected in the current model and left for future analysis. The proposed framework has been used to compute the attenuation coefficient and the power loss of the channel at different wavelengths in the visible spectrum, with the aim of showing the best choice according to the particular water conditions and the link characteristics. We demonstrate that the commonly adopted green light is not necessarily the best one, and that significant losses can originate from this suboptimal choice. Results also provide useful design guidelines for possible WDM configurations that minimise the effect of the impairments on the visible light propagation, by quantifying the available bandwidth to accommodate multiple adjacent channels with comparable losses.

The paper is structured as follows. In Section 2, the main effects that impact on the propagation of light in water are described for all the wavelengths in the visible spectrum as a function of the depth-dependent chlorophyll concentration, whereas in Section 3 we report results showing the attenuation suffered by visible light in different realistic water conditions, taking as a reference six wavelengths corresponding to different colours. Moreover, we extend the analysis to the whole visible light spectrum, thus identifying the available bandwidth for a WDM configuration, useful to ensure a higher data rate to the link. Finally, in Section 4 we draw some concluding remarks.

2 | Light Propagation in Water

2.1 | Chlorophyll Concentration

The performance of underwater communication links are significantly affected by chlorophyll concentration, which is the prevalent component of phytoplankton, a group of microorganisms characterising key elements of every water ecosystem. Phytoplankton rely on photosynthesis to obtain energy and, hence, they live in the surface layers of water (the so-called *photic zone*), and their concentration tends to decrease as the depth increases, due to the limited availability of sunlight to fuel their photosynthetic processes. Nonetheless, microorganisms also need nutrients, which are more easily available in deeper water. The deep chlorophyll maximum (DCM), which is a peak in chlorophyll concentration, represents the equilibrium between sunlight and nutrients, and it corresponds to the water layers with the highest presence of phytoplankton and chlorophyll. DCM's depth is typically between 15 and 120 m, depending on the surface concentration of chlorophyll and on the specific characteristics of the type of water [7, 9, 25].

The chlorophyll profile as a function of depth $C_c(z)$ can be modelled as a Gaussian curve which includes five numerically determined parameters. Its general form is defined as follows [7]:

$$C_c(z) = B_0 + Sz + \frac{h}{\sigma\sqrt{2\pi}} \exp\left[\frac{-(z - z_{max})^2}{2\sigma^2}\right] \quad (1)$$

where B_0 is the background chlorophyll concentration on the surface, S is the vertical gradient of concentration, which is always negative due to the slow decrease of $C_c(z)$ with depth, h is the total chlorophyll above the background levels, and z_{max} is the DCM depth. The standard deviation of the chlorophyll concentration, σ, is computed as[7]

$$\sigma = \frac{h}{\sqrt{2\pi}[C_c(z_{max}) - B_0 - Sz_{max}]}, \quad (2)$$

The parameters used in this paper to calculate (1) and (2) are reported in Table 1 for the *warm water* scenario [7]. The chlorophyll concentration C_c as a function of depth z obtained for two surface values, a low and a high one, that is $C_{surf} = 0.5$ mg/m^3 and $C_{surf} = 2$ mg/m^3, respectively, is shown in Figure 1. We notice that, as predicted by (1), the chlorophyll concentration exhibits a peak at a depth z_{max}, which will significantly impact the propagation of signals in the first metres of the communication link from surface to underwater. Obviously, the higher the surface chlorophyll concentration C_{surf}, the higher the overall chlorophyll concentration C_c at any depth.

TABLE 1 | Parameters of the considered *warm water* type [7].

	Surface chlorophyll concentration	
	$C_{surf} < 1$ mg/m^3	$C_{surf} \geq 1$ mg/m^3
B_0 (mg/m^3)	0.094	0.292
S (mg/m^4)	$-0.0087B_0 + 0.0004$	$-0.0052B_0 + 0.0002$
$C_c(z_{max})$ (mg/m^3)	$0.9C_{surf} + 0.334$	$1.03C_{surf} + 0.383$
h (mg/m^2)	$28.5C_c(z_{max}) + 23$	$28.5C_c(z_{max}) + 23$
z_{max} (m)	20	14.1

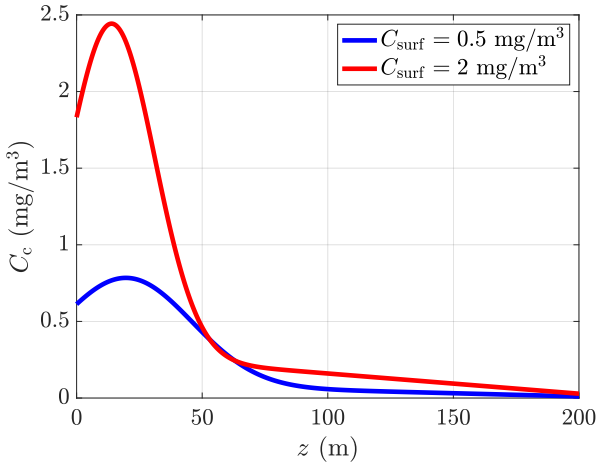

FIGURE 1 | Chlorophyll concentration versus depth for different values of the surface concentration C_{surf} in the *warm water* scenario in [7].

2.2 | Absorption, Scattering, Attenuation

Once the chlorophyll profile $C_c(z)$ has been quantified, it is possible to compute the attenuation coefficient

$$c(\lambda, z) = a(\lambda, z) + b(\lambda, z), \tag{3}$$

which is the sum of the wavelength- and depth-dependent coefficients for absorption $a(\lambda, z)$ and scattering $b(\lambda, z)$, being λ the wavelength of the transmitted light. The shape of absorption and scattering spectra depends on the contribution of different biological factors. For example, $a(\lambda, z)$ includes the absorption of pure water and of chlorophyll, which is the main substance that comprises phytoplankton, and the one of humic and fulvic acids, which are the nutrients for phytoplankton. The absorption spectrum is the sum of these contributions multiplied by their respective concentrations [9], that is

$$\begin{aligned} a(\lambda, z) = a_w(\lambda) &+ a_f^0 C_f(z)\exp(-k_f\lambda) \\ &+ a_h^0 C_h(z)\exp(-k_h\lambda) \\ &+ a_c^0(\lambda, z)\left(C_c(z)/C_c^0\right)^{0.602}, \end{aligned} \tag{4}$$

where $a_w(\lambda)$ is the (wavelength-dependent) pure water absorption coefficient (m^{-1}), a_f^0 is the specific absorption coefficient of fulvic acid, a_h^0 is the specific absorption coefficient of humic acid, $a_c^0(\lambda, z)$ is the (wavelength- and depth-dependent) specific absorption coefficient of chlorophyll (m^{-1}), $C_f(z)$ is the (depth-dependent) concentration of fulvic acid (mg/m^3), $C_h(z)$ is the (depth-dependent) concentration of humic acid (mg/m^3), k_f is the fulvic acid exponential coefficient, k_h is the humic acid exponential coefficient, and C_c^0 is a reference normalisation value (mg/m^3). The constant quantities, which are not affected by the wavelength, are reported in Table 2 [9]. The specific chlorophyll absorption can be computed using the following relation:

$$a_c^0(\lambda, z) = A(\lambda)C_c(z)^{-B(\lambda)}, \tag{5}$$

where $A(\lambda)$ and $B(\lambda)$ are empirical constants, whose list is available in ref. [27]. The values of these parameters for some significant wavelengths in the visible spectrum, corresponding to practically feasible lasers, are reported in Table 3 [26, 27].

The scattering spectrum is influenced by two main contributions: the first one is by pure water, and the second one by particulate substances, which can be divided into small and large particles, and have a different statistical distribution and strength. The complete equation for scattering spectrum is defined as follows [9]:

$$b(\lambda, z) = b_w(\lambda) + b_s^0(\lambda)C_s(z) + b_\ell^0(\lambda)C_\ell(z), \tag{6}$$

where $b_w(\lambda)$ is the (wavelength-dependent) pure water scattering coefficient (m^{-1}), $b_s^0(\lambda)$ is the (wavelength-dependent) scattering coefficient for small particulate matter (m^2/g), $b_\ell^0(\lambda)$ is the (wavelength-dependent) scattering coefficient for large particulate matter (m^2/g), $C_s(z)$ is the (depth-dependent) concentration of small particles (g/m^3), and $C_\ell(z)$ is the (depth-dependent) concentration of large particles (g/m^3). The wavelength dependencies for the scattering coefficients of pure water and of small and large particulate matter can be expressed as [9]

$$b_w(\lambda) = 0.005826\,(400/\lambda)^{4.322}, \tag{7}$$

$$b_s^0(\lambda) = 1.1513\,(400/\lambda)^{1.7}, \tag{8}$$

$$b_\ell^0(\lambda) = 0.3411\,(400/\lambda)^{0.3}. \tag{9}$$

Regarding the concentrations $C_f(z)$, $C_h(z)$, $C_s(z)$, and $C_\ell(z)$, needed to evaluate the previous equations, Haltrin proposed a simplified model to find the relationship between the concentrations of different particulates and the chlorophyll one [8]. These concentrations were determined numerically in terms of the chlorophyll one as

$$C_f(z) = 1.74098C_c(z)\exp(0.12327C_c(z)), \tag{10}$$

$$C_h(z) = 0.19334C_c(z)\exp(0.12343C_c(z)), \tag{11}$$

$$C_s(z) = 0.01739C_c(z)\exp(0.11631C_c(z)), \tag{12}$$

$$C_\ell(z) = 0.76284C_c(z)\exp(0.03092C_c(z)). \tag{13}$$

Notice that, from all these equations, if the chlorophyll concentration is known at any depth in the water, the absorption and scattering coefficients can be computed as well.

Figures 2a and 3a report the absorption coefficient $a(\lambda, z)$ calculated with (4), for the *warm water* with low and high value of C_{surf}, respectively. Different curves refer to results computed for specific colours, corresponding to possible operating wavelengths of the feasible light sources in the visible spectrum. We notice a peak at low depth in all the curves, which corresponds to the DCM in the C_c profile. Interestingly, the height of the peak varies for the different wavelengths. In particular, it is much more evident in the $a(\lambda, z)$ curve for shorter wavelengths, such as cyan, and especially blue. These light colours experience a significantly lower absorption with respect to red and orange, regardless of the water depth. For these longer wavelengths in the visible spectrum the peak in the absorption coefficient profile is less evident, being $a(\lambda, z)$ values high in all the positions underwater. This behaviour is due to the wavelength-specific parameters associated to water, reported in Table 3. Clearly, a higher chlorophyll concentration causes a higher absorption at any depth, regardless of the wavelength value.

Figures 2b and 3b show the scattering coefficient $b(\lambda, z)$ evaluated using (6) for the *warm water* [7] when chlorophyll at the water surface is low and high, respectively. Being strictly related to the chlorophyll concentration, also these curves present a peak at the depth corresponding to the maximum of $C_c(z)$. It is interesting to note that, unlike what happens for absorption, the shorter wavelengths of light, like the blue one, are more impaired by scattering than the longer ones, like the red one. Also in this case, as expected, larger values of the chlorophyll concentration result in higher scattering.

TABLE 2 | Additional parameters for the computation of absorption [9].

Parameter	Value
a_f^0	35.959 m^2/mg
a_h^0	18.828 m^2/mg
k_f	0.0189 nm^{-1}
k_h	0.01105 nm^{-1}
C_c^0	1 mg/m^3

TABLE 3 | Wavelength-specific absorption parameters of water [26, 27].

Colour	Wavelength (nm)	$a_w(\lambda)$ (m^{-1})	$A(\lambda)$	$B(\lambda)$
Blue	450	0.00922	0.0371	0.359
Cyan	492.5	0.0162	0.0267	0.356
Green	532.5	0.0447	0.0113	0.129
Yellow	575	0.0772	0.0052	0.018
Orange	605	0.2577	0.0055	0.082
Red	632.5	0.2995	0.0073	0.080

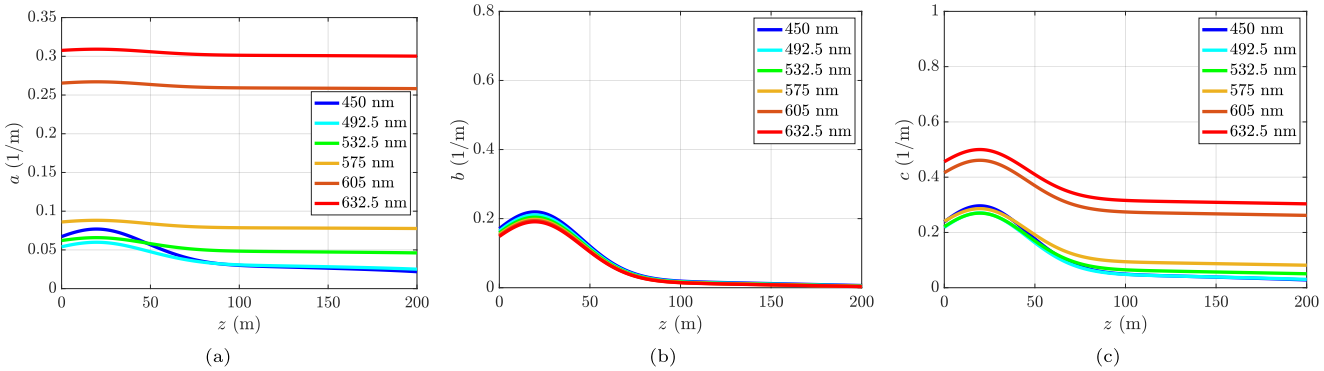

FIGURE 2 | (a) Absorption, (b) scattering, and (c) overall attenuation coefficients for *warm water* [7] with surface concentration $C_{\text{surf}} = 0.5$ mg/m^3, and different signal wavelengths.

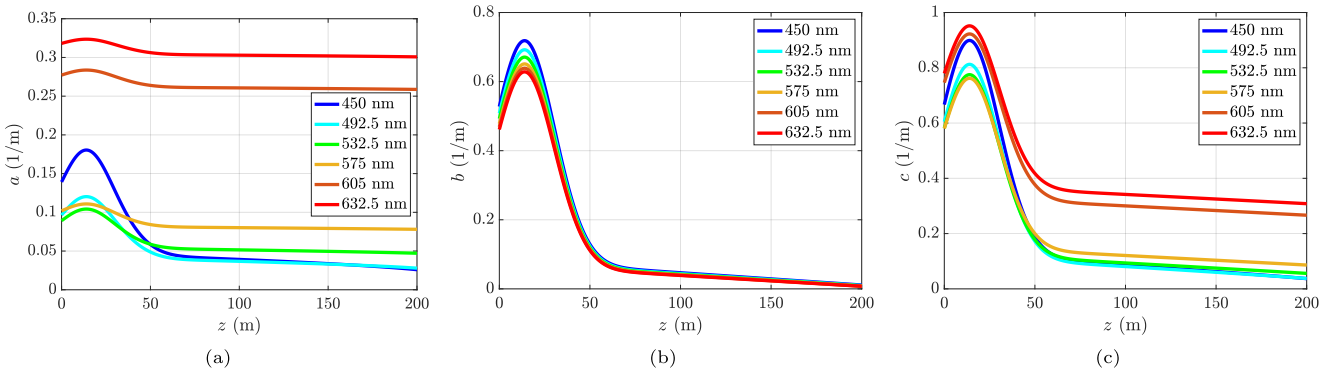

FIGURE 3 | (a) Absorption, (b) scattering, and (c) overall attenuation coefficients for *warm water* [7] with surface concentration $C_{\text{surf}} = 2$ mg/m^3, and different signal wavelengths.

Finally, Figures 2c and 3c depict the overall attenuation coefficient $c(\lambda, z)$, obtained for the same two *warm water types* [7] as described in (3), that is as the sum of absorption and scattering coefficients. As expected, also in this case the curves exhibit the peak at the DCM of the depth-dependent chlorophyll profile. We observe that orange and red are the most heavily impaired colours, while blue, cyan and green light presents the lowest attenuation coefficient. Notice that yellow light can represent an alternative to these colours for the light propagation in the first tens of metres beneath the surface, since it is more absorbed by water than blue and green light, but it is less affected by scattering. Moreover, as expected, higher C_{surf} values cause a significant attenuation increase for all wavelengths.

3 | Propagation Loss in UOWC Links

3.1 | Power Loss

The Beer–Lambert law states that the power of light propagating in a homogeneous medium decreases exponentially with a coefficient that is the product of the attenuation coefficient and the distance travelled [28]. If the medium is not homogeneous, as is water for a vertical UOWC link, its attenuation coefficient $c(\lambda, z)$ varies with depth and the power loss during light propagation can be calculated by integrating it over the distance covered. In this case, we can generalise the Beer–Lambert law as follows:

$$P(\lambda, z_r) = P_0 \exp\left\{ - \int_{\min(z_t, z_r)}^{\max(z_t, z_r)} c(\lambda, z) \mathrm{d}z \right\}, \tag{14}$$

where z_t is the transmitter depth, z_r is the receiver depth, P_0 is the initial power of the transmitted signal, and $c(\lambda, z)$ is the attenuation coefficient we described in the previous Section. Assuming a perfectly vertical path and normalising by P_0, Equation (14) can model the power loss of light in both uplink and down link scenarios. In contrast, if transmission is not exactly vertical, the length of the propagation path of light in the water has to be increased, taking into account a nonzero angle with respect to the vertical direction. Being the path longer, clearly the signal will lose more power. For the sake of simplicity, only vertical links have been considered in the present analysis.

Figure 4a,b shows the power loss computed in the *warm water* scenario [7] with the two values of the surface chlorophyll concentration considered in this analysis when a downlink transmission is taken into account, that is when the transmitter is placed at the water surface and the receiver is at a certain depth underwater. As we can notice, for the highest value of C_{surf}, the loss becomes extremely high after just a few tens of metres of depth. In particular, after the first 20 m underwater, the difference among the colours becomes more significant. The shortest wavelengths, especially cyan, green and yellow, become significantly less affected by loss going deeper underwater with respect to red and orange, whereas blue light has an intermediate behaviour in terms of loss. For the lowest chlorophyll surface value, the attenuation affecting visible light in its propagation underwater is much more limited, regardless of the wavelength. It is interesting to notice that, in both Figure 4a,b, the slope of the curves for light colours between cyan and yellow changes after a certain depth, which is shorter for the most turbid water. This means that the first segment of water, closer to the surface, is the most critical one for light propagation, which becomes much easier in deeper water, being less affected by scattering as shown in Figures 2b and 3b. This is due to the peak in the chlorophyll concentration arising at relatively low depth.

From this analysis, we can also draw some conclusions regarding the maximum possible receiver depth. In fact, assuming a transceiver scheme able to tolerate a maximum loss, the curves in Figure 4a,b can directly show us the maximum reachable depth. For example, if our communication scheme can support up to 75 dB of losses, we could place the receiver at a maximum depth of about 120 m in the lower chlorophyll concentration case, and at about 25 m when the chlorophyll concentration is higher. From the figures, we can also identify

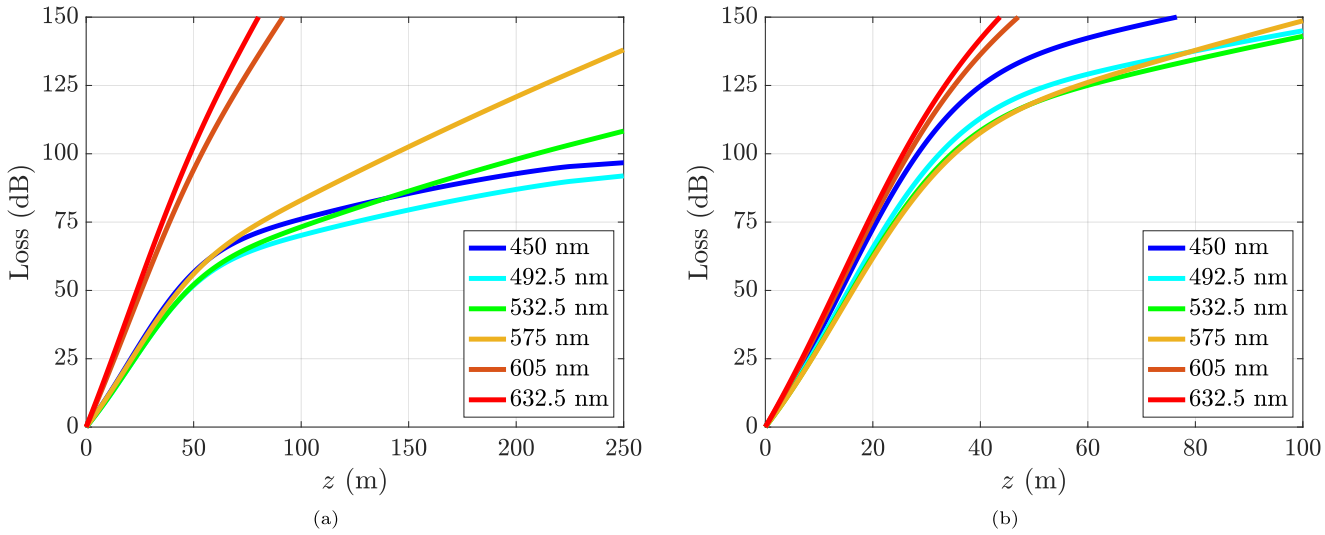

FIGURE 4 | Losses versus depth for *warm water* [7] with surface concentration (a) $C_{\text{surf}} = 0.5$ mg/m^3 and (b) $C_{\text{surf}} = 2$ mg/m^3, and different signal wavelengths in downlink transmission.

the transmission wavelength that should be adopted in the system to ensure the minimum losses, which would be cyan and yellow, respectively, for the considered example. In fact, we also notice that the optimal wavelength varies with both the depth and the chlorophyll concentration.

Another application of the proposed analysis is the study of underwater-to-underwater communication links using optical technology. We could imagine a scenario in which an underwater sensor network is composed of multiple nodes deployed at different depths. As we can see from Figure 4a,b, if the depth is higher than the DCM, losses are much lower than close to the surface. Hence, underwater nodes could exchange messages with each other with limited loss (i.e., needing a limited amount of power, a critical aspects in the nodes of sensor networks), exploiting the benefits of optical systems, such as high throughput and low latency. For example, we could lose just about 20 dB to transmit from 100 to 150 m in the lower chlorophyll case, and from 60 to 100 m in the higher chlorophyll scenario.

Similar observations can be referred to scenarios in which the transmitter is under water and the receiver is at the surface. Figure 5a,b refer to the case of a transmitter placed at 100 m under water, transmitting vertically upwards, in the two chlorophyll cases already considered. Clearly, also in this case, the most critical part of the link is the one closer to the surface, due to the presence of the DCM, while communication at higher depth experiences lower losses. For example, in the lower chlorophyll scenario, we would lose 25 dB to transmit from 100 to 40 m, but further 40 dB to reach the surface from a depth of 40 m.

If we compare downlink (Figure 4) and uplink cases (Figure 5), we notice that the behaviour of the losses is not symmetric. This depends on the behaviour of the chlorophyll concentration versus depth, which exhibits a peak in the DCM (see Figure 1). This peak is also present in the curves of $c(\lambda, z)$ (see Figures 2c and 3c). Clearly, the transmitted signal suffers a higher attenuation in correspondence of this peak. In the downlink scenario, the light signal passes first through the layers of water with the highest chlorophyll concentration, causing the highest loss values. For this reason, the slope of the curves in Figure 4 is higher in the first part, then it decreases, because light is passing through water layers with lower chlorophyll concentration and, as a consequence, lower attenuation. Vice versa, in the uplink case, we are considering a transmitter placed at a depth of 100 m. Hence, the signal crosses first layers of water with a low chlorophyll concentration, that means lower attenuation, and lower slope of the curves in Figure 5. Then, the chlorophyll concentration grows when the light reaches the layers of water around the DCM, thus causing a significant increase of the loss and of the slope of the curves in Figure 4.

3.2 | Available Bandwidth

The analysis performed in the previous section refers to some selected wavelengths in the visible spectrum, corresponding to feasible laser sources. If we extend the analysis to the whole visible spectrum, we can make additional remarks and considerations. Figure 6a,b represents the propagation losses as a function of the wavelength for the whole visible spectrum. The curves are computed for different values of the depth and the two figures refer to the two chlorophyll conditions already analysed previously. For each curve, the star highlights the optimal wavelength, that is, that which minimises the losses. The figures refer to vertical transmission from the surface to an underwater receiver, but similar conclusions can be drawn for the opposite scenario. Besides the obvious observation that losses are lower in the low chlorophyll case, we can notice some interesting effects, which can be summarised as follows:

- The optimal wavelength is basically steady at 500 nm for $C_{\text{surf}} = 0.5$ mg/m^3, but it tends to decrease, from 560 to 500 nm, as the depth increases, when $C_{\text{surf}} = 2$ mg/m^3. This is consistent with the fact that 500 nm is the best choice when the water is not too turbid (relatively low chlorophyll concentration), if we observe that the chlorophyll concentration decreases as the depth increases.

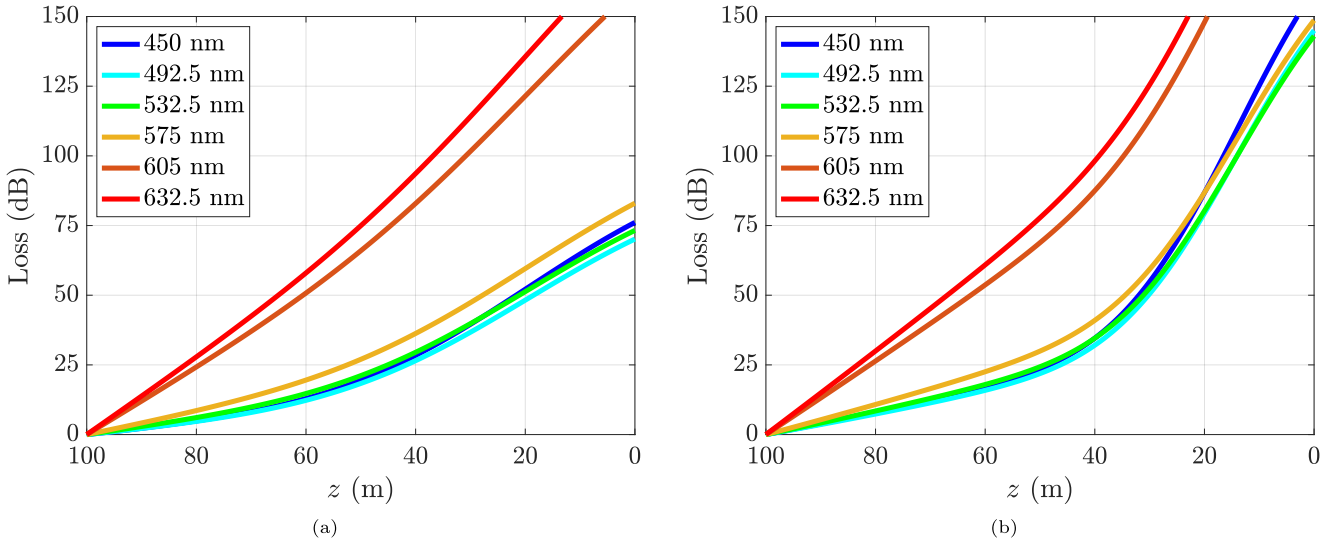

FIGURE 5 | Losses versus depth for *warm water* [7] with surface concentration (a) $C_{\text{surf}} = 0.5$ mg/m^3 and (b) $C_{\text{surf}} = 2$ mg/m^3, and different signal wavelengths in uplink transmission.

- There is a region, around the optimal wavelength, in which the losses are practically constant.

This last observation can be exploited to define a *minimum-loss wavelength range*, in which we could allocate several channels in a wavelength division multiplexing way, to ensure a higher capacity of the communication link. Figure 7a,b represent the *3-dB bandwidth* of the channel, defined as the range of wavelengths for which the losses are within 3 dB from the minimum loss, corresponding to the optimal wavelength, at each depth. We highlight the upper and lower limits of the bandwidth and the optimal bandwidth. Clearly, when the depth is very small, the bandwidth tends to infinity due to the almost total absence of losses in the very first part of the link. Nonetheless, in the low chlorophyll case we can observe that the bandwidth tends to decrease until a depth of about 70 m, then it remains practically constant, about 50 nm wide. The behaviour when the chlorophyll concentration is higher is similar, although the available bandwidth decreases faster, and the optimal wavelength fluctuates more, as we could also conclude from Figure 6b. Finally, Figure 8 compares the available bandwidth for the two considered chlorophyll concentrations. We notice that, in general, a lower chlorophyll concentration ensures a larger available bandwidth.water.

4 | Conclusions

In this paper, we considered the propagation of light in a vertical underwater optical wireless communication link. We analysed the main effects affecting visible light propagation in water as a function of depth, by highlighting the depth-dependent variations of absorption, scattering, and attenuation in scenarios based on realistic water characteristics. We first considered six wavelengths in the visible spectrum, corresponding to feasible laser sources, and showed that some

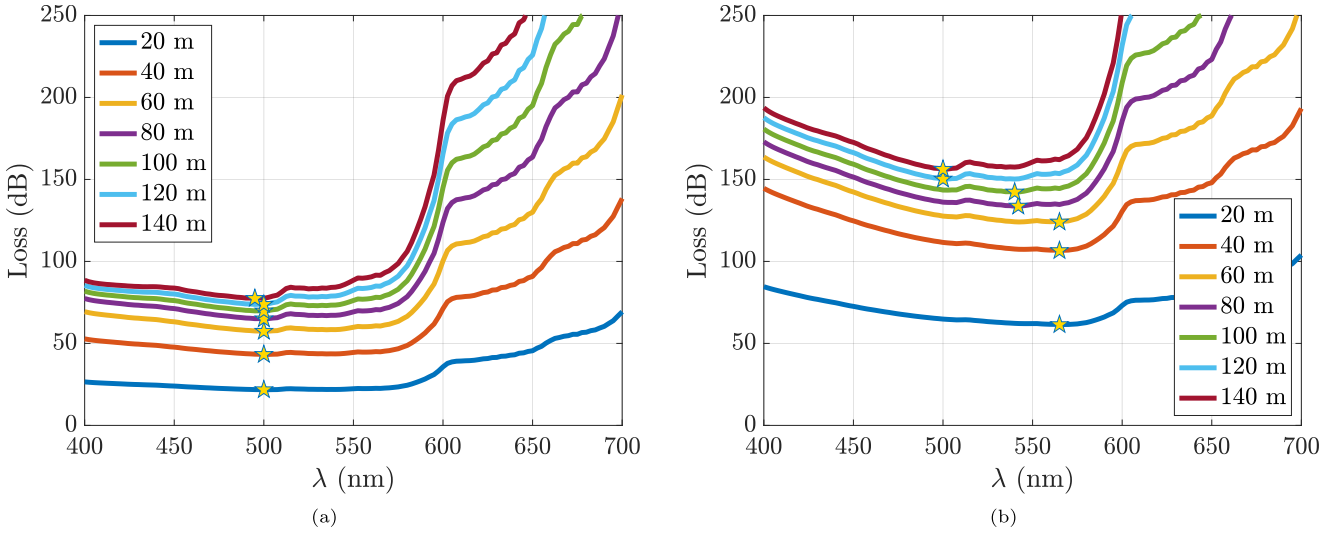

FIGURE 6 | Losses versus wavelength for *warm water* [7] with surface concentration (a) $C_{\text{surf}} = 0.5$ mg/m^3 and (b) $C_{\text{surf}} = 2$ mg/m^3, and different receiver depths.

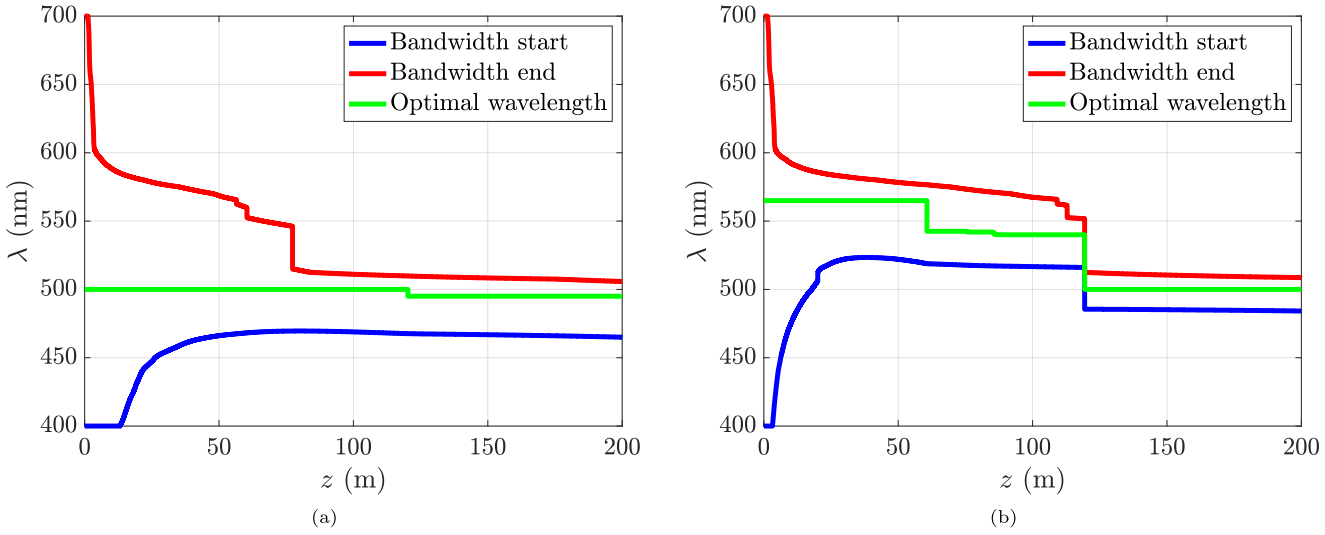

FIGURE 7 | Bandwidth versus depth for *warm water* [7] with surface concentration (a) $C_{\text{surf}} = 0.5$ mg/m^3 and (b) $C_{\text{surf}} = 2$ mg/m^3.

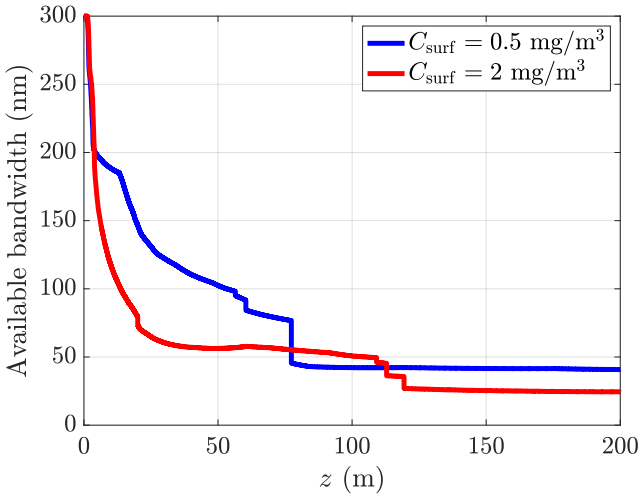

FIGURE 8 | Bandwidth comparison for *warm water* [7] with different surface concentration as a function of depth.

wavelengths are more suitable than others due to the wavelength-dependent variations of the water parameters. We evaluated the power losses experienced by a signal transmitted from the surface towards the bottom of the sea and vice versa, highlighting similarities and differences between the two links. In particular, we showed that the section of water closer to the surface is the most critical one, suggesting also the feasibility of some possible underwater-to-underwater communication scenarios, and the identification of the maximum transmitter or receiver depth for a given acceptable power loss level.

Finally, we defined and computed the available bandwidth by evaluating power losses over the whole visible spectrum. We demonstrated that there exist regions of contiguous wavelengths which can be exploited to accommodate multiple channels in order to improve the system capacity. We could notice that the optimal transmission wavelengths are around green when the water is not too turbid and tend to shift towards yellow as the turbidity increases.

The work presented in this paper can lead to the identification of the best transmission window in underwater optical wireless communications, which is fundamental for a proper system design and necessary to define a correct link budget and performance analysis in future underwater systems.

Author Contributions

All authors contributed to the design of the study. The conceptualization, methodology, and formal analysis were performed by Alessandro Ugolini and Federica Poli. The first draft of the manuscript was written by Alessandro Ugolini and Federica Poli, and the review and editing of the draft version were carried out by all authors. Funding was acquired by all authors. All authors read and approved the final manuscript.

Acknowledgements

This work was supported by the European Space Agency under the framework of SatNEx V project. The view expressed herein can in no way be taken to reflect the official opinion of the European Space Agency. Open access publishing facilitated by Università degli Studi di Parma, as part of the Wiley - CRUI-CARE agreement.

Conflicts of Interest

The authors declare no conflicts of interest.

Data Availability Statement

The authors have nothing to report.

References

1. H. Kaushal and G. Kaddoum, "Underwater Optical Wireless Communication," *IEEE Access* 4 (April 2016): 1518–1547, https://doi.org/10.1109/access.2016.2552538.

2. Z. Zeng, S. Fu, H. Zhang, Y. Dong, and J. Cheng, "A Survey of Underwater Optical Wireless Communications," *IEEE communications Surveys & Tutorials* 19, no. 1 (2017): 204–238, https://doi.org/10.1109/comst.2016.2618841.

3. L. K. Chen, Y. Shao, and Y. Di, "Underwater and Water-Air Optical Wireless Communication," *Journal of Lightwave Technology* 40, no. 5 (2022): 1440–1452, https://doi.org/10.1109/jlt.2021.3125140.

4. C. W. Chow, "Recent Advances and Future Perspectives in Optical Wireless Communication, Free Space Optical Communication and Sensing for 6G," *Journal of Lightwave Technology* 42, no. 11 (June 2024): 3972–3980, https://doi.org/10.1109/jlt.2024.3386630.

5. B. M. Cochenour, L. J. Mullen, and A. E. Laux, "Characterization of the Beam-Spread Function for Underwater Wireless Optical Communications Links," *IEEE Journal of Oceanic Engineering* 33, no. 4 (2008): 513–521, https://doi.org/10.1109/joe.2008.2005341.

6. C. Gabriel, M. A. Khalighi, S. Bourennane, P. Leon, and V. Rigaud, "Monte-Carlo-based Channel Characterization for Underwater Optical Communication Systems," *IEEE/OSA Journal of Optical Communications and Networking* 5, no. 1 (2013): 1–12, https://doi.org/10.1364/jocn.5.000001.

7. T. Kameda and S. Matsumura, "Chlorophyll Biomass off Sanriku, Northwestern Pacific, Estimated by Ocean Color and Temperature Scanner (OCTS) and a Vertical Distribution Model," *Journal of Oceanography* 54, no. 5 (September 1998): 509–516, https://doi.org/10.1007/bf02742452.

8. V. I. Haltrin, "Chlorophyll-Based Model of Seawater Optical Properties," *Applied Optics* 38, no. 33 (November 1999): 6826–6832, https://doi.org/10.1364/ao.38.006826.

9. L. J. Johnson, R. J. Green, and M. S. Leeson, "Underwater Optical Wireless Communications: Depth Dependent Variations in Attenuation," *Applied Optics* 52, no. 33 (November 2013): 7867–7873, https://doi.org/10.1364/ao.52.007867.

10. I. C. Ijeh, M. A. Khalighi, M. Elamassie, S. Hranilovic, and M. Uysal, "Outage Probability Analysis of a Vertical Underwater Wireless Optical Link Subject to Oceanic Turbulence and Pointing Errors," *Journal of Optical Communications and Networking* 14, no. 6 (June 2022): 439–453, https://doi.org/10.1364/jocn.454191.

11. X. Ke, S. Yang, Y. Sun, J. Liang, and X. Pan, "Underwater Blue-Green LED Communication Using a Double-Layered, Curved Compound-Eye Optical System," *Optics Express* 30, no. 11 (May 2022): 18599–18616, https://doi.org/10.1364/oe.457052.

12. K. Zhang, C. Sun, W. Shi, et al., "Turbidity-Tolerant Underwater Wireless Optical Communications Using Dense Blue–Green Wavelength Division Multiplexing," *Optics Express* 32, no. 12 (June 2024): 20762–20775, https://doi.org/10.1364/oe.521575.

13. L. J. Johnson, R. J. Green, and M. S. Leeson, "Underwater Optical Wireless Communications: Depth-Dependent Beam Refraction,"

Applied Optics 53, no. 31 (November 2014): 7273–7277, https://doi.org/10.1364/ao.53.007273.

14. J. Hong, J. Zou, Y. Wang, et al., "All-Fiber Cyan Laser at 491.5 nm," *Optics Letters* 48, no. 5 (March 2023): 1327–1330, https://doi.org/10.1364/ol.483830.

15. M. P. Lord, L. Talbot, M. Bernier, and R. Vallée, "Monolithic Silica Fiber Laser Operating at 585 nm," *Optics Letters* 48, no. 2 (January 2023): 514–517, https://doi.org/10.1364/ol.480592.

16. J. Zou, J. Hong, Z. Zhao, et al., "3.6 W Compact All-Fiber Pr^{3+}-Doped Green Laser at 521 nm," *Advanced Photonics* 4, no. 5 (2022): 056001, https://doi.org/10.1117/1.ap.4.5.056001.

17. M. Kong, W. Lv, T. Ali, et al., "10-m 9.51-Gb/s RGB Laser Diodes-Based WDM Underwater Wireless Optical Communication," *Optics Express* 25, no. 17 (August 2017): 20829–20834, https://doi.org/10.1364/oe.25.020829.

18. R. S. Keiffer, J. C. Novarini, and G. V. Norton, "The Impact of the Background Bubble Layer on Reverberation-Derived Scattering Strengths in the Low to Moderate Frequency Range," *Journal of the Acoustical Society of America* 97, no. 1 (January 1995): 227–234, https://doi.org/10.1121/1.412990.

19. A. Ugolini, F. Poli, D. Croce, and S. Mangione, "Characterization of Depth-Dependent Loss for Visible Light Propagation in Underwater Optical Wireless Links," in *2024 Italian Conference on Optics and Photonics (ICOP)* (IEEE, 2024), 1–4, https://doi.org/10.1109/ICOP62013.2024.10803631.

20. N. Anous, M. Abdallah, M. Uysal, and K. Qaraqe, "Performance Evaluation of LOS and NLOS Vertical Inhomogeneous Links in Underwater Visible Light Communications," *IEEE Access* 6 (2018): 22408–22420, https://doi.org/10.1109/access.2018.2815743.

21. X. Quan and E. S. Fry, "Empirical Equation for the Index of Refraction of Seawater," *Applied Optics* 34, no. 18 (June 1995): 3477–3480, https://doi.org/10.1364/ao.34.003477.

22. M. Elamassie and M. Uysal, "Performance Characterization of Vertical Underwater VLC Links in the Presence of Turbulence," in *2018 11th International Symposium on Communication Systems, Networks and Digital Signal Processing (CSNDSP)* (IEEE, 2018), 1–6, https://doi.org/10.1109/CSNDSP.2018.8471888.

23. M. Elamassie, S. M. Sait, and M. Uysal, "Effect of Sea Waves on Vertical Underwater Visible Light Communication Links," *IEEE Journal of Oceanic Engineering* 48, no. 2 (2023): 515–525, https://doi.org/10.1109/joe.2022.3211286.

24. M. Elamassie and M. Uysal, "Vertical Underwater VLC Links Over Cascaded Gamma-Gamma Turbulence Channels With Pointing Errors," in *2019 IEEE International Black Sea Conference on Communications and Networking (BlackSeaCom)* (IEEE, 2019): 1–5, https://doi.org/10.1109/BlackSeaCom.2019.8812811.

25. J. Uitz, H. Claustre, A. Morel, and S. B. Hooker, "Vertical Distribution of Phytoplankton Communities in Open Ocean: An Assessment Based on Surface Chlorophyll," *Journal of Geophysical Research: Oceans (San Francisco)* 111, no. C8 (2006), https://doi.org/10.1029/2005jc003207.

26. R. M. Pope and E. S. Fry, "Absorption Spectrum (380–700 nm) of Pure Water. II. Integrating Cavity Measurements," *Applied Optics* 36, no. 33 (November 1997): 8710–8723, https://doi.org/10.1364/ao.36.008710.

27. A. Bricaud, M. Babin, A. Morel, and H. Claustre, "Variability in the Chlorophyll-Specific Absorption Coefficients of Natural Phytoplankton: Analysis and Parameterization," *Journal of Geophysical Research: Oceans (San Francisco)* 100, no. C7 (1995): 13321–13332, https://doi.org/10.1029/95jc00463.

28. M. C. A. Naboulsi, H. Sizun, and F. de Fornel, "Wavelength Selection for the Free Space Optical Telecommunication Technology," in *Reliability of Optical Fiber Components, Devices, Systems, and Networks II*, eds. H. G. Limberger and M. J. Matthewson, 5465 (International Society for Optics and Photonics. SPIE, 2004), 168–179.